iScience

CellPress

Article

Solution-Deposited Solid-State Electrochromic Windows

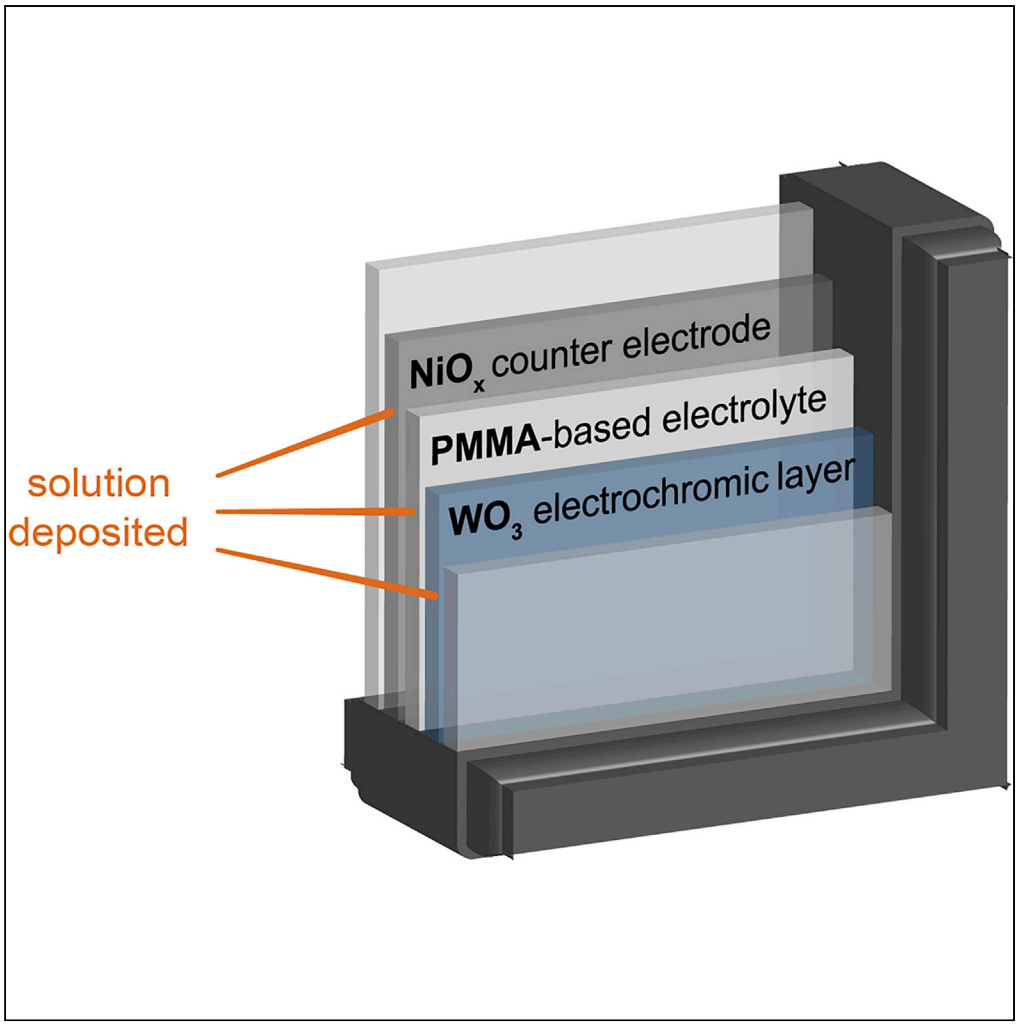

Wei Cheng, Marta Moreno-Gonzalez, Ke Hu, ..., David M. Weekes, Brian Tam, Curtis P. Berlinguette

cberling@chem.ubc.ca

HIGHLIGHTS

Amorphous WO_3 and NiO_x films are produced by a solution-deposition method

The WO_3 and NiO_x films are assembled into a solid-state electrochromic device

The solid-state device exhibits state-of-the-art electrochromic performance

Amorphous NiO_x is a superior counter electrode material compared with crystalline NiO_x

Cheng et al., iScience *10*, 80–86
December 21, 2018
https://doi.org/10.1016/j.isci.2018.11.014

iScience

CellPress

Article

Solution-Deposited Solid-State Electrochromic Windows

Wei Cheng,[1] Marta Moreno-Gonzalez,[1] Ke Hu,[2,3] Caroline Krzyszkowski,[1,3] David J. Dvorak,[3] David M. Weekes,[1] Brian Tam,[1] and Curtis P. Berlinguette[1,2,3,4,*]

SUMMARY

Commercially available electrochromic (EC) windows are based on solid-state devices in which WO_3 and NiO_x films commonly serve as the EC and counter electrode layers, respectively. These metal oxide layers are typically physically deposited under vacuum, a time- and capital-intensive process when using rigid substrates. Herein we report a facile solution deposition method for producing amorphous WO_3 and NiO_x layers that prove to be effective materials for a solid-state EC device. The full device containing these solution-processed layers demonstrates performance metrics that meet or exceed the benchmark set by devices containing physically deposited layers of the same compositions. The superior EC performance measured for our devices is attributed to the amorphous nature of the NiO_x produced by the solution-based photodeposition method, which yields a more effective ion storage counter electrode relative to the crystalline NiO_x layers that are more widely used. This versatile method yields a distinctive approach for constructing EC windows.

INTRODUCTION

Electrochromic (EC) windows (also known as smart or dynamic windows) undergo changes in light transmittance in response to an applied voltage, enabling the dynamic control of daylight and solar heat passing through buildings (Granqvist, 2006, 2012a; Runnerstrom et al., 2014). This technology can provide both indoor thermal and visual comfort for building occupants while improving building energy efficiency by as much as 20% (Granqvist, 2012a). These features have prompted substantial investment into deploying EC windows at scale, but the high price of such windows ($1,000/m^2 *c.f.* ~$150/m^2 for a regular window (Smart windows cost, 2016)) has prevented their widespread use. A significant fraction of the cost is imbedded in the vacuum environment required to sputter EC window layers. This process can require a substantial capital outlay, and the long residence times needed to fabricate the key layers on rigid substrates also preclude rapid throughput (Garg et al., 2005). These factors present the impetus to develop solution-based deposition methodologies to reduce the costs associated with fabricating EC windows (Barile et al., 2017; Cai et al., 2016a; Llordés et al., 2016).

A conventional EC window consists of an EC layer, an electrolyte layer, and an ion storage counter electrode sandwiched between two transparent conducting layers (Figure 1). Thin films of WO_3 and NiO_x are widely used as the respective EC and counter electrode layers in commercial EC windows (Gillaspie et al., 2010; Niklasson and Granqvist, 2006). Both of these layers contribute to reversible color switching in response to an electrical bias (Figure 1). The NiO_x layers are lithiated to form Li_yNiO_x before device assembly to provide a source of intercalating Li^+ during reduction (coloration) of WO_3. A voltage applied to the assembled device drives coloration of both metal oxide layers as Li^+ migrates into the WO_3 layer. The ion-conducting and electrically insulating electrolyte layer serves to shuttle Li^+ between the metal oxide layers and prevent short circuiting of the device. Liquid electrolytes are common in academic studies, but solid polymer-based electrolytes are used in commercial systems to satisfy safety and sealing issues (Granqvist, 2012b; Thakur et al., 2012).

The EC behavior of these layers is exquisitely sensitive to impurities, film defects, thickness, porosity, and crystallinity (Cai et al., 2016b; Granqvist, 2014; Lee et al., 2006; Scherer and Steiner, 2013). These factors therefore impose very stringent conditions on how EC windows can be manufactured. Physical vacuum deposition has emerged as the most reliable and scalable method of producing uniform and optical-quality metal oxide films of variable thicknesses (Thummavichai et al., 2017). Notwithstanding, the metal oxide semiconductor industry teaches that manufacturing methods progressively transition from vacuum to solution-processing methods to reduce costs (Yu et al., 2016). The ability to solution process at ambient

[1]Department of Chemistry, The University of British Columbia, 2036 Main Mall, Vancouver, BC V6T 1Z1, Canada

[2]Department of Chemical and Biological Engineering, The University of British Columbia, 2360 East Mall, Vancouver, BC V6T 1Z3, Canada

[3]Stewart Blusson Quantum Matter Institute, The University of British Columbia, 2355 East Mall, Vancouver, BC V6T 1Z4, Canada

[4]Lead Contact

*Correspondence: cberling@chem.ubc.ca

https://doi.org/10.1016/j.isci.2018.11.014

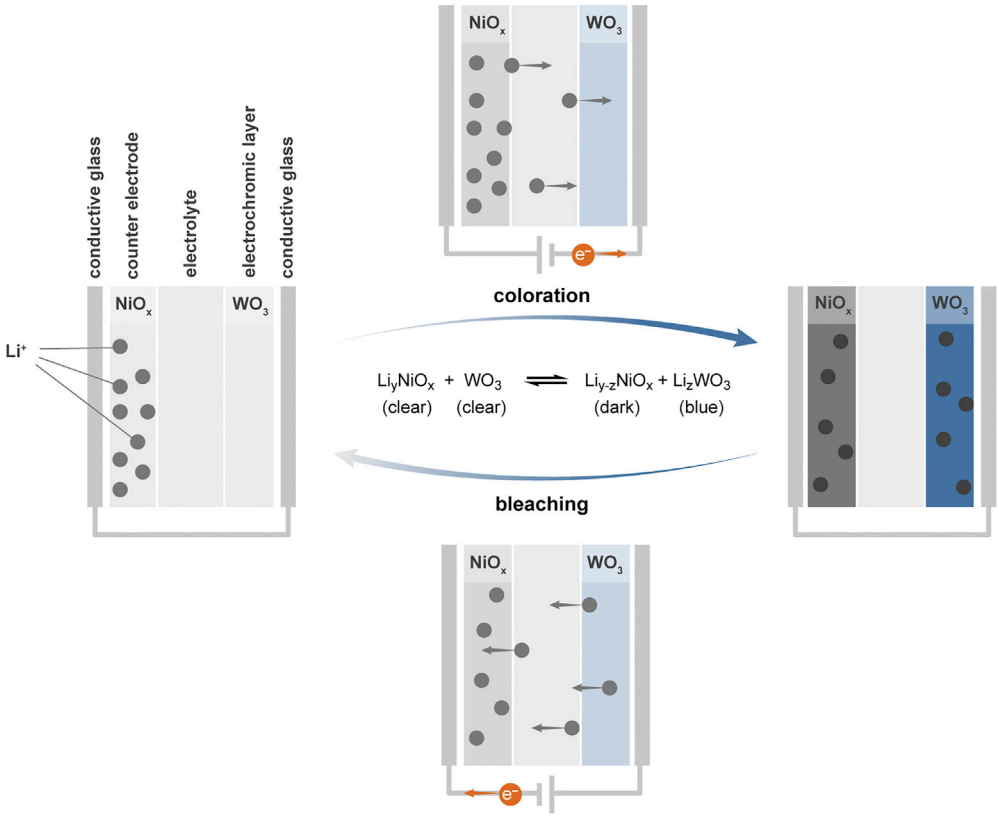

Figure 1. Working Principles for an Electrochromic Device

Scheme outlining the coloration and bleaching process of an EC device with a WO_3 electrochromic layer and NiO_x counter electrode layer sandwiched between two transparent conductive glass substrates. The pristine device is formed by transparent Li_yNO_x and WO_3 layers and an interstitial electrolyte. Applying a forward bias to the electrochromic layer of the device injects electrons into WO_3, which are then compensated by Li^+ migrating from the counter electrode through the electrolyte to yield colored Li_xWO_3. The simultaneous extrusion of Li^+ from Li_yNiO_x enables the formation of colored $Li_{y-z}NO_x$. The bleaching process is obtained by applying a reverse bias, yielding the initial Li_yNiO_x and WO_3 transparent layers. The coloration and bleaching processes are summarized by the overall reversible reaction shown in the Scheme.

temperatures and pressures offers the opportunity to reduce energy consumption and capital equipment while also reducing processing times (Llordés et al., 2016). Moreover, the avoidance of high vacuum lessens the safety concerns associated with handling potentially hazardous materials (e.g., lithium-containing chemicals). There are several reports of solution-based methods for processing EC or counter electrode layers, including electrodeposition (Baeck et al., 2003; Cai et al., 2016b), chemical bath deposition (Ristova et al., 2002; Vidales-Hurtado and Mendoza-Galván, 2008; Xia et al., 2008), sol-gel methods (Livage and Ganguli, 2001), and spray pyrolysis (Kamal et al., 2005; Tenent et al., 2010). However, none of these methods are well suited for synthesizing *both* WO_3 and NiO_x films. Consequently, these layers are evaluated in electrochemical half-cells or in devices in which the working or counter electrode is physically deposited (Jiao et al., 2003; Srivastava et al., 2005; Zhang et al., 2009). These observations motivated us to build an EC device wherein all layers are solution-processed.

We demonstrate herein the use of a "photodeposition" method (Cheng et al., 2018; Smith et al., 2013) to solution-process both the WO_3 and NiO_x EC layers of an EC device with a solution-deposited poly(methyl methacrylate) (PMMA)-based electrolyte. To our knowledge, this is the first report of a solid-state EC device containing internal layers that are fully solution-processable at low temperature. The performance of our laboratory-scale solid-state EC devices meets or exceeds current literature benchmarks in terms of optical modulation ($\Delta T_{633\ nm}$; measured as the difference in light transmittance between the fully colored and bleached states at $\lambda = 633$ nm), switching time for coloration (t_{color}; defined by the time required to reach 90% of a transmittance change from the fully bleached to fully colored state) and bleaching (t_{bleach}), and

Counter Electrode Material	Phase	Deposition Method	ΔT (%)	t_{color} (s)	t_{bleach} (s)	CE (cm^2/C)	Reference
NiO porous film	Crystalline	Chemical bath deposition	55	10	20	87.2	Zhang et al., 2009 [a]
NiO nanoparticle film	Crystalline	Inkjet printing	75	10	13	131.9	Cai et al., 2016a [b]
NiO_x film	Crystalline	Magnetron sputtering	52	5	2	–	Liu et al., 2016 [c]
NiO_x film	Amorphous	Photodeposition	60	4	6	141	this work[d]
NiO_x film	Crystalline	Photodeposition	26	78	17	72	this work[d]

Table 1. Performance Parameters of Our Solid-State EC Devices in Comparison with That of Solid-State Devices Reported in the Literature
All devices use WO_3 as the electrochromic layer, NiO_x as the counter electrode, and a polymer-based electrolyte.
[a]Measured at 633 nm over the −2.5 to +2.5 V potential range.
[b]Measured at 550 nm over the −2.5 to +2.5 V potential range.
[c]Measured at 550 nm over the −1.8 to +1.8 V potential range.
[d]Measured at 633 nm over the −2.1 to +2.1 V potential range.

coloration efficiency (CE; the change in optical density acquired by injection of charge per unit area; Table 1). We also demonstrate the superior performance of amorphous thin film materials in EC windows by directly comparing amorphous and crystalline NiO_x counter electrodes in the same device architecture and produced by analogous solution-based methods. This study presents an opportunity to harness low-cost solution-processing methods for the production of high quality EC devices.

RESULTS AND DISCUSSION

Electrode Synthesis and Device Assembly

Amorphous tungsten oxide (a-WO_3) films were prepared using a photodeposition methodology known to yield amorphous metal oxide layers (Cheng et al., 2018; He et al., 2017; Smith et al., 2013). Briefly, a solution of WCl_6 in 2-propanol was spin-cast onto a fluorine-doped tin oxide (FTO) substrate and the resultant precursor film was irradiated with UV light (λ_{max} = 185 nm) to form a metal oxide film. Characterization of the films by top-view and cross-sectional scanning electron microscopy (SEM) was consistent with the successful formation of porous a-WO_3 films of ~600 nm thickness (Figure S1). NiO_x films were prepared following a similar procedure: aqueous solutions of 0.25 M $NiCl_2$ were spin-cast onto an FTO substrate followed by UV irradiation (λ_{max} = 185 nm) for 8 hr. The complete liberation of chlorine from the precursor film and the formation of NiO_x was confirmed by X-ray fluorescence and X-ray photoelectron spectroscopy analyses (Figure S2). The X-ray diffraction (XRD) pattern of the as-prepared NiO_x films showed a broad reflection centered at $2\theta = 18^\circ$ indexed to the (001) facets of α-$Ni(OH)_2$ (Smith et al., 2016), together with the reflections corresponding to the FTO substrate (Figure S3). This broad reflection was no longer observed, and no additional reflections appeared after annealing the NiO_x films at 200°C for 1 hr, which denotes the successful formation of amorphous films (Figure S3). The thickness of a-NiO_x films prepared by spin casting and UV treating five layers of $NiCl_2$ precursor on the FTO substrate before the annealing step was determined to be 120 nm by cross-sectional SEM (Figure 2). Cross-sectional and top-view SEM images (Figures 2 and S4A) show that the NiO_x films follow the contour of FTO and have smooth uniform surfaces. Crystalline NiO_x (c-NiO_x) films were also obtained by annealing the as-deposited NiO_x films at 400°C for 1 hr. The resulting XRD pattern shows well-defined reflections corresponding to crystalline cubic NiO (Figure S3). Five-layer c-NiO_x films show smooth uniform surfaces with a thickness of 105 nm (Figures S4B and S4C).

Solid-state EC devices with active areas of ~2 cm^2 were assembled using a-WO_3 films coated on FTO glass as the working electrode, either a- or c-NiO_x films deposited on FTO glass as the counter electrode, and a PMMA-based gel as the electrolyte. NiO_x counter electrodes were lithiated before device assembly by submerging the films in 1 M $LiClO_4$ propylene carbonate and applying a potential of −1.5 V (vs Ag/AgCl) across the cell for 5 min. The PMMA-based gel electrolyte was drop-cast directly onto the a-NiO_x electrode and contained within a silicone spacer with a thickness of 1 mm. The device was completed with the a-WO_3 working electrode and sealed with epoxy glue.

Electrochromic Performance of Solid-State Devices

The EC performance of the full devices containing either a- or c-NiO_x counter electrode was tested by using UV-Vis spectroscopy to measure the optical properties under applied potentials (Figure 3). The optical

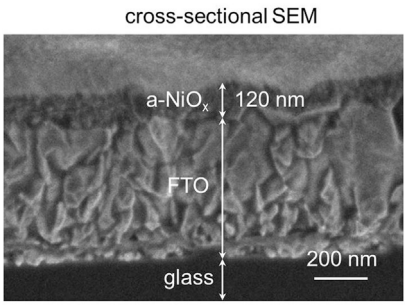

Figure 2. SEM Characterization of Amorphous NiO_x Films
Cross-sectional SEM images of five-layer a-NiO_x films produced by photodeposition followed by annealing at 200°C for 1 hr. Cross-sectional SEM images were acquired on fresh edges of cleaved samples at a tilt angle of 52°. See also Figures S1–S4, S6, and S7.

modulation ($\Delta T_{633\ nm}$) was determined by recording the transmittance of the devices in either a fully colored or a fully bleached state at potentials of −2.1 or +2.1 V, respectively. EC devices with the a-NiO_x counter electrode showed a $\Delta T_{633\ nm}$–60%, compared with $\Delta T_{633\ nm}$–26% for the device with c-NiO_x counter electrode (Figure 3A) (*c.f.* 19% for devices in which the counter electrode was bare FTO [Figure S5]). Switching times from the fully colored to the fully bleached state (t_{bleach}), and the reverse (t_{color}), were measured by tracking the transmittance at λ = 633 nm in response to consecutive applied potentials of +2.1 and −2.1 V for 30 s each (Figure 3B). The device with the a-NiO_x counter electrode showed rapid switching times of $t_{bleach} \sim 6$ s and $t_{color} \sim 4$ s, whereas the device with a c-NiO_x counter electrode showed much slower t_{color} and t_{bleach} of 78 and 17 s, respectively.

CE, which measures the change in optical density acquired by injection of charge per unit area, was determined in accordance with Equations 1 and 2:

$$CE = \frac{\Delta(OD)}{\Delta Q} \quad \text{(Equation 1)}$$

$$\Delta(OD) = \log\left(\frac{T_b}{T_c}\right) \quad \text{(Equation 2)}$$

where Δ(OD) is the change in optical density and ΔQ is the charge density (C/cm^2) obtained from electrochemical measurements; T_b is the maximum transmittance in the bleached state at a fixed wavelength (obtained from Figure 3B); and T_c is the varying transmittance obtained during the coloration process at this same wavelength. The CE values derived from the slope of the linear region of Δ(OD) versus ΔQ (Figure 3C) were determined to be 141 cm^2/C for a device containing an a-NiO_x counter electrode. This value is approximately twice that of the device with c-NiO_x counter electrode (72 cm^2/C).

The differences in performance metrics of the EC devices containing either an a-NiO_x or c-NiO_x counter electrode demonstrate the superior EC performance of a-NiO_x systems. It appears that the superior performance of a-NiO_x is manifest in the superior ion-storage properties of the films given that a-NiO_x is characterized by a charge capacity of 4.1 mC/cm^2 during the pre-lithiation process that is 2-fold higher than the value measured for c-NiO_x (1.6 mC/cm^2). These findings are consistent with the higher ion storage capacity generally observed for amorphous materials (Ku et al., 2012; Lee et al., 2014). The improved ion storage performance that arises in amorphous materials is believed to be due to the larger interstitial spaces between more disordered atoms (Lee et al., 2014; Legrain et al., 2015; Llordés et al., 2016). These larger interatomic spaces can accommodate intercalated ions and facilitate the mobility of ions in materials. In the case of NiO_x counter electrode materials in EC devices, the amorphous film is capable of balancing more charges during each EC cycle, thereby accommodating greater lithium insertion into the WO_3 during each coloration cycle and resulting in higher ΔT. Furthermore, the enhanced ion mobility in a-NiO_x yields faster switching times between bleach and colored states.

Table 1 lists the performance of our solid-state EC devices containing photodeposited NiO_x counter electrodes along with other reported devices of similar sizes and configurations. The $\Delta T_{633\ nm}$ of 60% reported here for the a-NiO_x is in keeping with systems synthesized by other methods. The switching times (t_{bleach} and t_{color}) of our device is among the fastest reported to date, exceeded only by t_{bleach} for films made using high-vacuum sputtering methods. The CE of 141 cm^2/C exceeds all other known examples of devices based on WO_3 and NiO_x materials, highlighting the excellent EC performance of our solution-processed

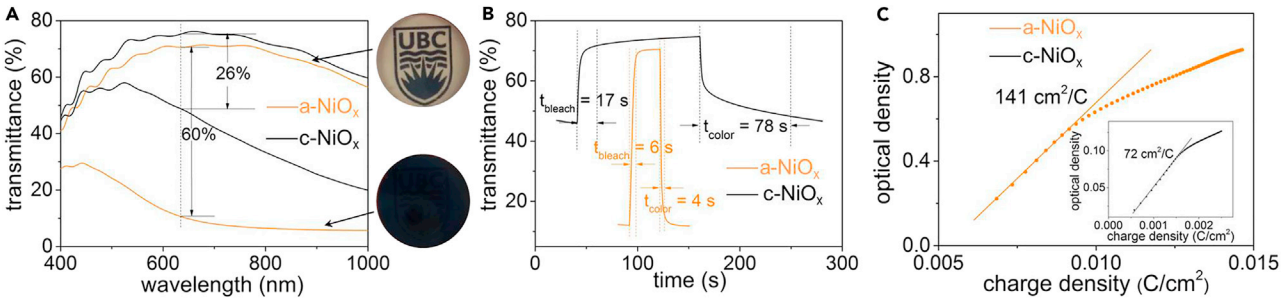

Figure 3. Amorphous NiO_x Layers Make Superior Counter Electrodes

(A) Transmittance spectra of EC devices using a-NiO_x (orange trace) and c-NiO_x (black trace) as counter electrodes at colored and bleached states. The spectra were recorded after coloring at −2.1 V or bleaching at +2.1 V for 60 s. The images are the solid-state device using a-NiO_x as counter electrode in bleached and colored states.

(B) Transmittance change at wavelength of 633 nm for the EC devices with a-NiO_x (orange trace) and c-NiO_x (black trace) on FTO as counter electrode as a function of time. The devices were bleached at +2.1 V for 30 s, then colored at −2.1 V for another 30 s. Switching times t_{color} and t_{bleach} are indicated.

(C) Changes in optical density of the devices using a-NiO_x and c-NiO_x (inset) on FTO as counter electrode at 633 nm as a function of charge density. Coloration efficiency values were determined by fitting the linear region of the plot (Equation 1 and 2).

See also Figures S5, S8, and S9.

devices containing amorphous films. It is worth noting that the performance is also comparable with commercially available EC windows, which use sputtered WO_3 and NiO_x films and polymer-based electrolytes. These full-scale windows typically show an optical modulation of merely ~45% over the visible light region and a switching time of 15–20 min (with the important caveat that the device sizes are different) (Range of products, 2018).

Performance Dependence on a-NiO_x Thickness

The thicknesses of the a-NiO_x films are controlled simply by spin casting and UV treating a variable number of $NiCl_2$ precursor layers on the FTO substrate before annealing. NiO_x films with thicknesses of 70, 120, 240, and 360 nm were prepared by 3, 5, 10, or 15 layers of deposition, respectively (Figures 2, S6, and S7). Amorphous NiO_x films of increasing thicknesses (120, 240, and 360 nm) were assembled into EC devices as the counter electrode material (with all other parameters held constant) and similarly assessed for their optical properties in response to an applied voltage. Increasing thickness of a-NiO_x from 120 nm to 360 nm caused a slight decrease in $\Delta T_{633\ nm}$ from 60% to 56% (Figure S8). Switching times t_{bleach} and t_{color} also increased slightly reaching 11 and 13 s, respectively, for the thickest of the three a-NiO_x films (Figure S8). The stability of the EC devices was also tested by tracking the transmittance change over time while continuously switching between the colored and bleached states. The thicker NiO_x films exhibit enhanced cycling stability despite the loss in optical modulation and increase in switching times. SEM characterization showed that the 120-nm a-NiO_x film was compromised during cycling, whereas the morphologies of the thicker films (240 and 360 nm) were mostly maintained (Figure S9). For the device with a 120-nm thickness of a-NiO_x, 81% of the initial optical modulation value remained after 100 cycles (Figure 4A). The EC device with a 240-nm thickness of a-NiO_x retained 90% of the initial ΔT after 100 cycles and 75% after 200 cycles (Figure 4B). Further increasing the thickness of the a-NiO_x film to 360 nm enabled the device to retain nearly 100% of the initial ΔT after 400 cycles (Figure 4C). By contrast, solid-state devices using inkjet-printed WO_3 and NiO nanoparticle electrodes retain only 80% $\Delta T_{633\ nm}$ after 100 cycles, with significant further degradation thereafter (Cai et al., 2016a).

Conclusion

Solution-based photodeposition of readily available metal precursors (WCl_6 and $NiCl_2$) can be used to synthesize both the working and counter electrode materials of EC windows. The exceptional performance of EC devices containing these materials is demonstrated here with amorphous WO_3 and NiO_x thin films assembled together with a PMMA-based gel electrolyte. The resulting solid-state systems exhibit optical modulations ($\Delta T_{633\ nm}$), switching times (t_{color} and t_{bleach}), coloration efficiencies (CE), and cycling stabilities commensurate with the best reported devices to date, including those produced by expensive or specialized methods. We also show that this low-temperature process yields amorphous layers of NiO_x that act as

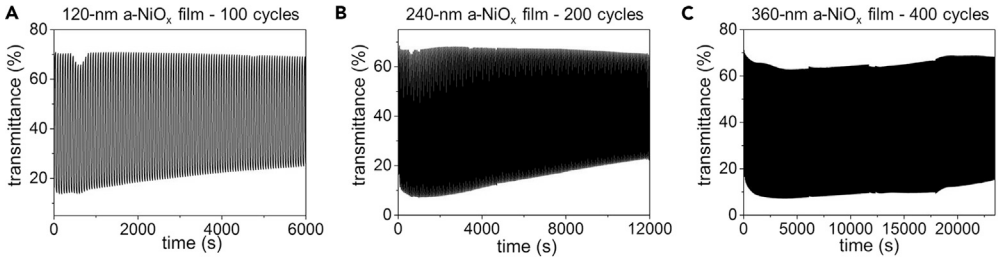

Figure 4. Thickness-Dependent Electrochromic Cycling Stability

(A–C) Transmittance changes at wavelength of 633 nm as a function of time during the electrochromic switching between colored and bleached states for EC devices using a-NiO_x films with thicknesses of (A) 120 nm, (B) 240 nm, and (C) 360 nm as counter electrodes. In each electrochromic cycle, the devices were held at potential −2.1 V for 30 s then switched to +2.1 V for another 30 s.

See also Figure S8.

superior counter electrodes relative to crystalline NiO_x, which we anticipate will trigger greater research efforts on the use of amorphous materials for EC devices. These collective results represent an opportunity to drive down the costs of energy-saving EC windows that have already attracted substantial commercial investment.

Limitations of the Study

This study demonstrates the ability to use photodeposition to make uniform EC nickel and tungsten oxide layers. The formation of the photodeposited a-NiO_x films must be optimized to compete with sputtering at an industrial scale. Future investigations will also seek to resolve the factors that lead to the increases in transmittance of the bleached state during cycling (Figure 4C).

METHODS

All methods can be found in the accompanying Transparent Methods supplemental file.

SUPPLEMENTAL INFORMATION

Supplemental Information includes Transparent Methods and 9 figures and can be found with this article online at https://doi.org/10.1016/j.isci.2018.11.014.

ACKNOWLEDGMENTS

The authors are grateful to the Canadian Natural Science and Engineering Research Council (RGPIN 337345-13), Canadian Foundation for Innovation (229288), Canadian Institute for Advanced Research (BSE-BERL-162173), Canada Research Chairs, and Stewart Blusson Quantum Matter Institute for financial support. Additional thanks to the Center for High-Throughput Phenogenomics for access to SEM facilities. D.M.W. and C.P.B. also wish to acknowledge the generous and ongoing support of Peter Bradshaw.

AUTHOR CONTRIBUTIONS

C.P.B. supervised the project. W.C. designed and performed the experiments. M.M. carried out XRD measurements. D.J.D. conducted SEM analyses. K.H., C.K., and B.T. assisted with thin film preparation. W.C., D.M.W., and C.P.B. wrote the manuscript with input from all authors.

DECLARATION OF INTERESTS

The authors declare no competing interests.

Received: August 25, 2018
Revised: October 21, 2018
Accepted: November 6, 2018
Published: December 21, 2018

REFERENCES

Baeck, S.-H., Choi, K.-S., Jaramillo, T.F., Stucky, G.D., and McFarland, E.W. (2003). Enhancement of photocatalytic and electrochromic properties of electrochemically fabricated mesoporous WO_3 thin films. Adv. Mater. *15*, 1269–1273.

Barile, C.J., Slotcavage, D.J., Hou, J., Strand, M.T., Hernandez, T.S., and McGehee, M.D. (2017). Dynamic windows with neutral color, high contrast, and excellent durability using reversible metal electrodeposition. Joule *1*, 133–145.

Cai, G., Darmawan, P., Cui, M., Chen, J., Wang, X., Eh, A.L.-S., Magdassi, S., and Lee, P.S. (2016a). Inkjet-printed all solid-state electrochromic devices based on NiO/WO_3 nanoparticle complementary electrodes. Nanoscale *8*, 348–357.

Cai, G., Cui, M., Kumar, V., Darmawan, P., Wang, J., Wang, X., Lee-Sie Eh, A., Qian, K., and Lee, P.S. (2016b). Ultra-large optical modulation of electrochromic porous WO_3 film and the local monitoring of redox activity. Chem. Sci. *7*, 1373–1382.

Cheng, W., He, J., Dettelbach, K.E., Johnson, N.J.J., Sherbo, R.S., and Berlinguette, C.P. (2018). Photodeposited amorphous oxide films for electrochromic windows. Chem *4*, 821–832.

Garg, D., Henderson, P.B., Hollingsworth, R.E., and Jensen, D.G. (2005). An economic analysis of the deposition of electrochromic WO_3 via sputtering or plasma enhanced chemical vapor deposition. Mater. Sci. Eng. B *119*, 224–231.

Gillaspie, D.T., Tenent, R.C., and Dillon, A.C. (2010). Metal-oxide films for electrochromic applications: present technology and future directions. J. Mater. Chem. *20*, 9585–9592.

Granqvist, C.-G. (2006). Electrochromic materials: out of a niche. Nat. Mater. *5*, 89–90.

Granqvist, C.G. (2012a). Oxide electrochromics: an introduction to devices and materials. Sol. Energy Mater. Sol. Cells *99*, 1–13.

Granqvist, C.G. (2012b). Electrochromic device. World patent WO2012138281A1.

Granqvist, C.G. (2014). Electrochromics for smart windows: oxide-based thin films and devices. Thin Solid Films *564*, 1–38.

He, J., Weekes, D.M., Cheng, W., Dettelbach, K.E., Huang, A., Li, T., and Berlinguette, C.P. (2017). Photodecomposition of metal nitrate and chloride compounds yields amorphous metal oxide films. J. Am. Chem. Soc. *139*, 18174–18177.

Jiao, Z., Wu, M., Qin, Z., and Xu, H. (2003). The electrochromic characteristics of sol–gel-prepared NiO thin film. Nanotechnology *14*, 458.

Kamal, H., Elmaghraby, E.K., Ali, S.A., and Abdel-Hady, K. (2005). The electrochromic behavior of nickel oxide films sprayed at different preparative conditions. Thin Solid Films *483*, 330–339.

Ku, J.H., Ryu, J.H., Kim, S.H., Han, O.H., and Oh, S.M. (2012). Reversible lithium storage with high mobility at structural defects in amorphous molybdenum dioxide electrode. Adv. Funct. Mater. *22*, 3658–3664.

Lee, S.-H., Deshpande, R., Parilla, P.A., Jones, K.M., To, B., Mahan, A.H., and Dillon, A.C. (2006). Crystalline WO_3 nanoparticles for highly improved electrochromic applications. Adv. Mater. *18*, 763–766.

Lee, J., Urban, A., Li, X., Su, D., Hautier, G., and Ceder, G. (2014). Unlocking the potential of cation-disordered oxides for rechargeable lithium batteries. Science *343*, 519–522.

Legrain, F., Malyi, O., and Manzhos, S. (2015). Insertion energetics of lithium, sodium, and magnesium in crystalline and amorphous titanium dioxide: a comparative first-principles study. J. Power Sources *278*, 197–202.

Liu, Q., Dong, G., Xiao, Y., Delplancke-Ogletree, M.-P., Reniers, F., and Diao, X. (2016). Electrolytes-relevant cyclic durability of nickel oxide thin films as an ion-storage layer in an all-solid-state complementary electrochromic device. Sol. Energy Mater. Sol. Cells *157*, 844–852.

Livage, J., and Ganguli, D. (2001). Sol–gel electrochromic coatings and devices: a review. Sol. Energy Mater. Sol. Cells *68*, 365–381.

Llordés, A., Wang, Y., Fernandez-Martinez, A., Xiao, P., Lee, T., Poulain, A., Zandi, O., Saez Cabezas, C.A., Henkelman, G., and Milliron, D.J. (2016). Linear topology in amorphous metal oxide electrochromic networks obtained via low-temperature solution processing. Nat. Mater. *15*, 1267–1273.

Niklasson, G.A., and Granqvist, C.G. (2006). Electrochromics for smart windows: thin films of tungsten oxide and nickel oxide, and devices based on these. J. Mater. Chem. *17*, 127–156.

(2018). Range of products | EControl-Glas GmbH und Co. KG. Available at: https://www.econtrol-glas.de/en/knowledge-center/range-of-products.

Ristova, M., Velevska, J., and Ristov, M. (2002). Chemical bath deposition and electrochromic properties of NiO_x films. Sol. Energy Mater. Sol. Cells *71*, 219–230.

Runnerstrom, E.L., Llordés, A., Lounis, S.D., and Milliron, D.J. (2014). Nanostructured electrochromic smart windows: traditional materials and NIR-selective plasmonic nanocrystals. Chem. Commun. (Camb.) *50*, 10555–10572.

Scherer, M.R.J., and Steiner, U. (2013). Efficient electrochromic devices made from 3D nanotubular gyroid networks. Nano Lett. *13*, 3005–3010.

(2016).Smart Windows Cost-How Much Does Smart Glass Cost? - Modernize. Available at: https://modernize.com/home-ideas/32437/smart-windows-cost.

Smith, R.D.L., Prévot, M.S., Fagan, R.D., Zhang, Z., Sedach, P.A., Siu, M.K.J., Trudel, S., and Berlinguette, C.P. (2013). Photochemical route for accessing amorphous metal oxide materials for water oxidation catalysis. Science *340*, 60–63.

Smith, R.D.L., Sherbo, R.S., Dettelbach, K.E., and Berlinguette, C.P. (2016). On how experimental conditions affect the electrochemical response of disordered nickel oxyhydroxide films. Chem. Mater. *28*, 5635–5642.

Srivastava, A.K., Deepa, M., Singh, S., Kishore, R., and Agnihotry, S.A. (2005). Microstructural and electrochromic characteristics of electrodeposited and annealed WO_3 films. Solid State Ionics *176*, 1161–1168.

Tenent, R.C., Gillaspie, D.T., Miedaner, A., Parilla, P.A., Curtis, C.J., and Dillon, A.C. (2010). Fast-switching electrochromic Li^+ -doped NiO Films by ultrasonic spray deposition. J. Electrochem. Soc. *157*, H318–H322.

Thakur, V.K., Ding, G., Ma, J., Lee, P.S., and Lu, X. (2012). Hybrid materials and polymer electrolytes for electrochromic device applications. Adv. Mater. *24*, 4071–4096.

Thummavichai, K., Xia, Y., and Zhu, Y. (2017). Recent progress in chromogenic research of tungsten oxides towards energy-related applications. Prog. Mater. Sci. *88*, 281–324.

Vidales-Hurtado, M.A., and Mendoza-Galván, A. (2008). Optical and structural characterization of nickel oxide-based thin films obtained by chemical bath deposition. Mater. Chem. Phys. *107*, 33–38.

Xia, X.H., Tu, J.P., Zhang, J., Wang, X.L., Zhang, W.K., and Huang, H. (2008). Electrochromic properties of porous NiO thin films prepared by a chemical bath deposition. Sol. Energy Mater. Sol. Cells *92*, 628–633.

Yu, X., Marks, T.J., and Facchetti, A. (2016). Metal oxides for optoelectronic applications. Nat. Mater. *15*, 383–396.

Zhang, J., Tu, J.P., Xia, X.H., Qiao, Y., and Lu, Y. (2009). An all-solid-state electrochromic device based on NiO/WO_3 complementary structure and solid hybrid polyelectrolyte. Sol. Energy Mater. Sol. Cells *93*, 1840–1845.

ISCI, Volume *10*

Supplemental Information

Solution-Deposited Solid-State Electrochromic Windows

Wei Cheng, Marta Moreno-Gonzalez, Ke Hu, Caroline Krzyszkowski, David J. Dvorak, David M. Weekes, Brian Tam, and Curtis P. Berlinguette

Supplemental Figures

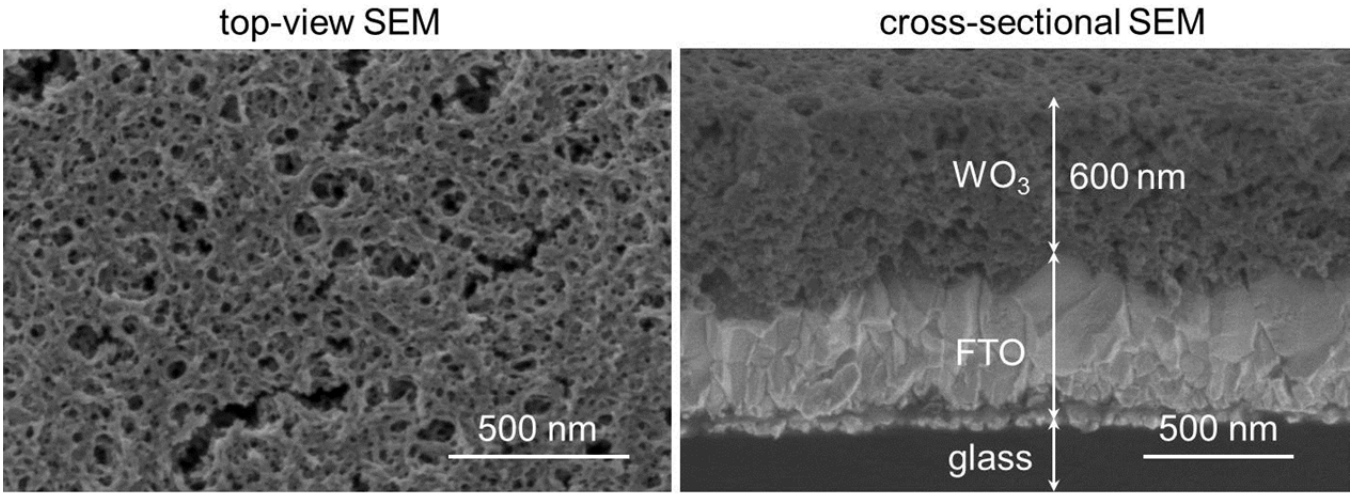

Figure S1. SEM characterization of a-WO_3 films, Related to Figure 2. Top-view (left) and cross-sectional (right) SEM images of 5-layer WO_3 films produced by photodeposition followed by annealing at 100°C for 1 hr. Cross-sectional SEM images were acquired on fresh edges of cleaved samples at a tilt angle of 52 degrees.

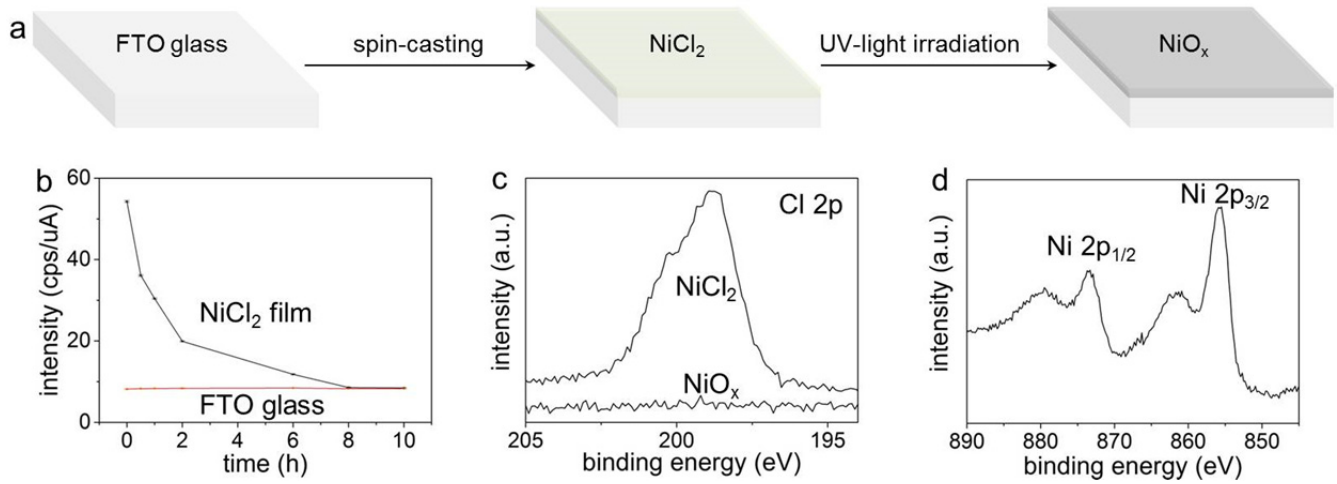

Figure S2. Photodeposition of NiO_x films, Related to Figure 2. (a) Schematic illustration showing UV light irradiation of spin-cast $NiCl_2$ precursor films on FTO glass leads to formation of NiO_x. (b) Content of Cl in precursor film determined by X-ray fluorescence (XRF) analyzer as a function of UV irradiation time. The chloride ions are completely removed by UV light illumination in 8 hrs. (c) XPS spectra of $NiCl_2$ precursor and as-formed NiO_x in binding energy range corresponding to Cl 2p. No Cl 2p signal exists in as-formed NiO_x, confirming complete decomposition of chloride ions by UV irradiation. (d) XPS spectrum of NiO_x in the binding energy range corresponding to Ni 2p, matching well with that of Ni^{2+}.

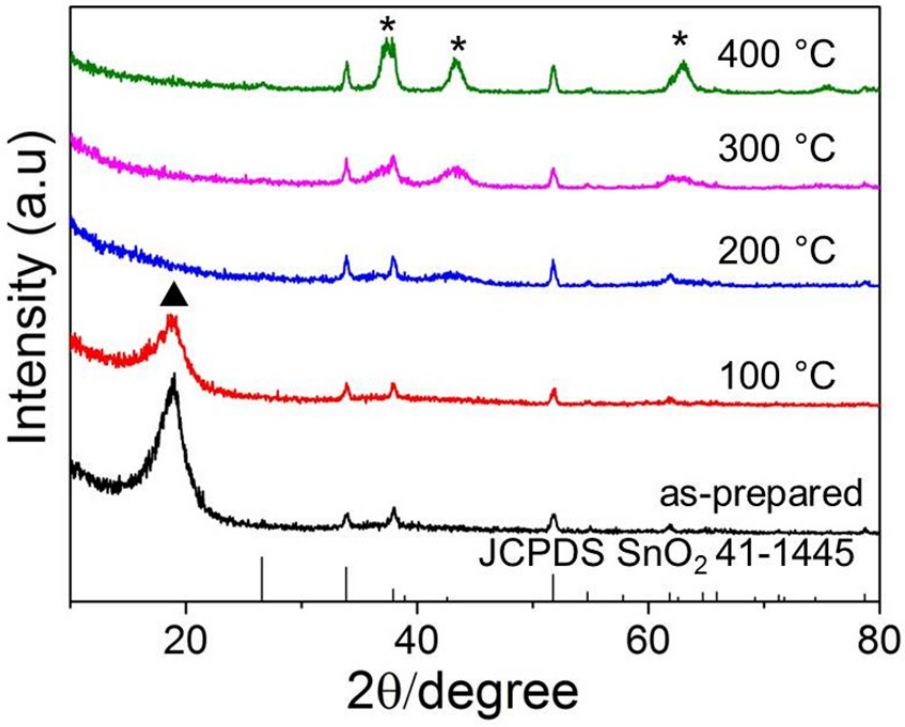

Figure S3. XRD characterization, Related to Figure 2. XRD patterns of photodeposited NiO_x films annealed at 100, 200, 300, and 400°C for 1 hr. Broad diffraction peak at labeled with ▲ symbol corresponds to (100) planes of α-$Ni(OH)_2$. The reflections denoted with * symbol correspond to cubic phase NiO (JCPDS 47-1049). All other reflections arising from the FTO substrate can be indexed to SnO_2 (JCPDS 41-1445).

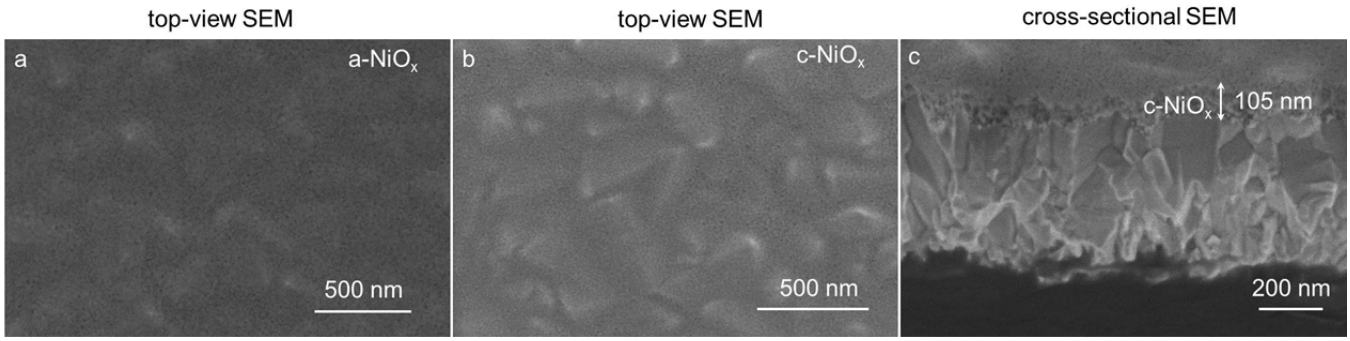

Figure S4. SEM characterization of amorphous and crystalline NiO_x films, Related to Figure 2. (a, b) Top-view and (c) cross-sectional SEM images of a- and c-NiO_x films produced by photodeposition followed by annealing at 200 and 400°C for 1 hr, respectively. Cross-sectional SEM images were acquired on fresh edges of cleaved samples at a tilt angle of 52 degrees.

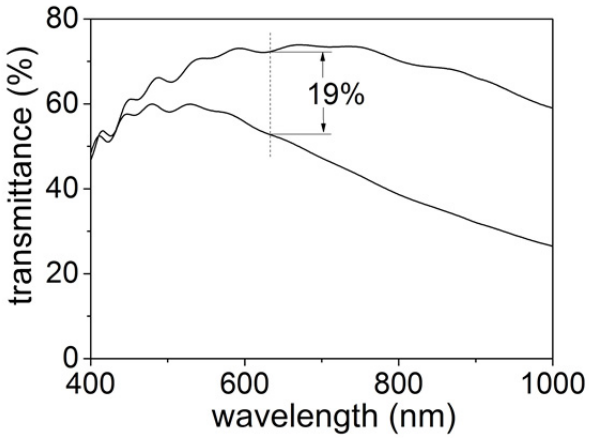

Figure S5. Optical modulation of an EC device with bare FTO counter electrode, Related to Figure 3. Transmittance spectra of EC device using bare FTO as the counter electrode in the colored and bleached states. The spectra were recorded after coloring at -2.1 V or bleaching at +2.1 V for 60 s. $\Delta T_{633\ nm}$ was determined to be 19%.

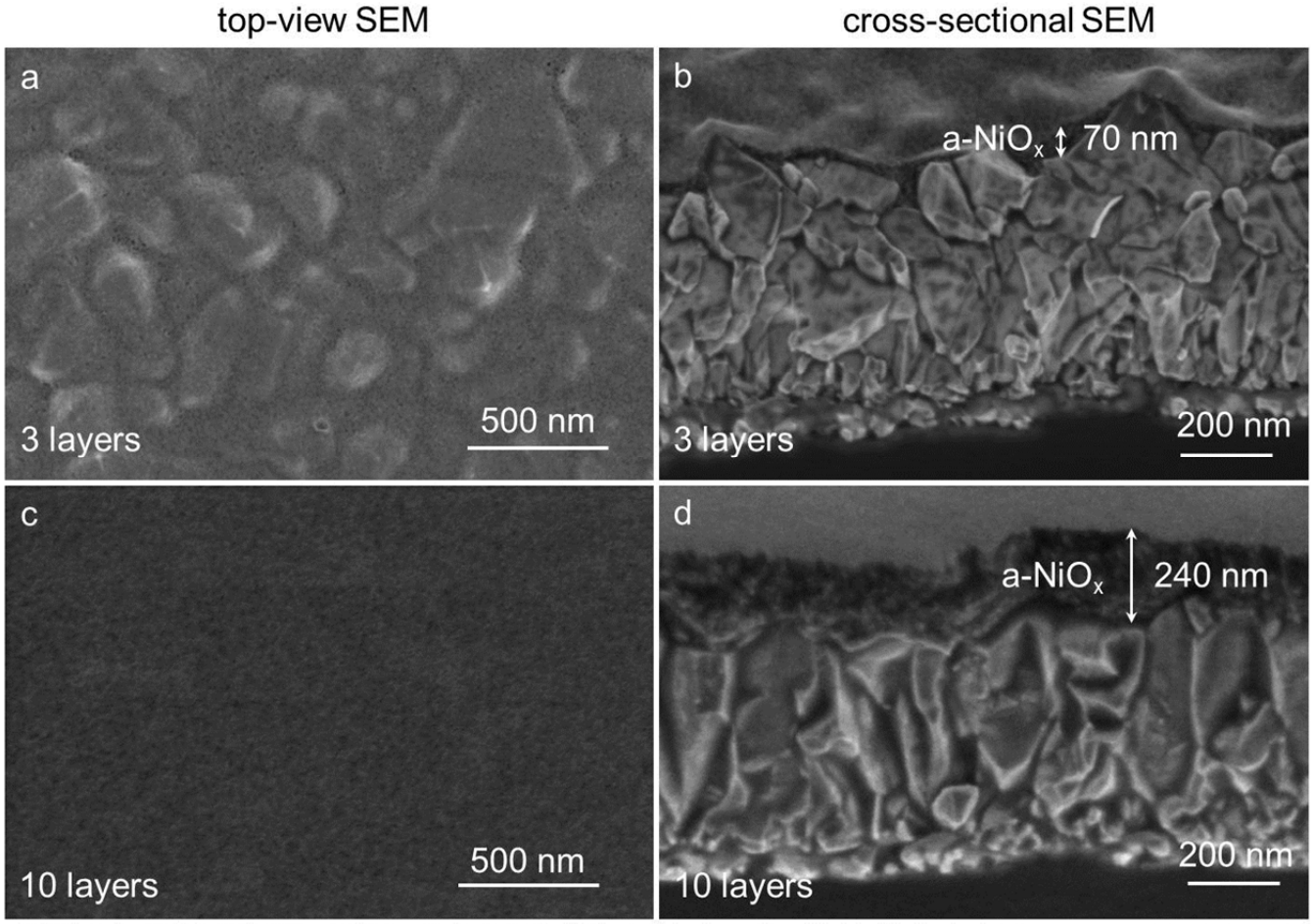

Figure S6. SEM characterization of a-NiO_x film, Related to Figure 2. (a, c) Top-view and (b, d) cross-sectional SEM images of 3-layer and 10-layer a-NiO_x films produced by photodeposition followed by annealing at 200°C for 1 hr. Cross-sectional SEM images were acquired on fresh edges of cleaved samples at a tilt angle of 52 degrees.

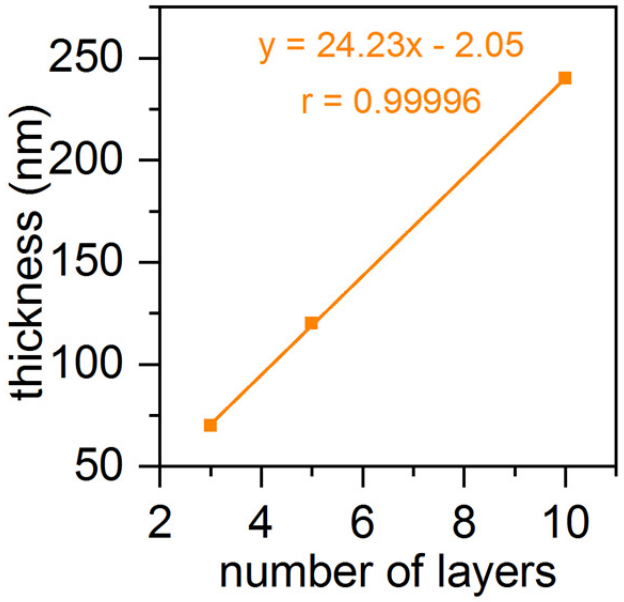

Figure S7. Relation between film thickness and number of deposition layers, Related to Figure 2. A linear relation was found between the thickness of a-NiO_x films determined from cross-sectional SEM images (see Figures 2 and S6) and the number of layers of a-NiO_x coated on FTO substrates.

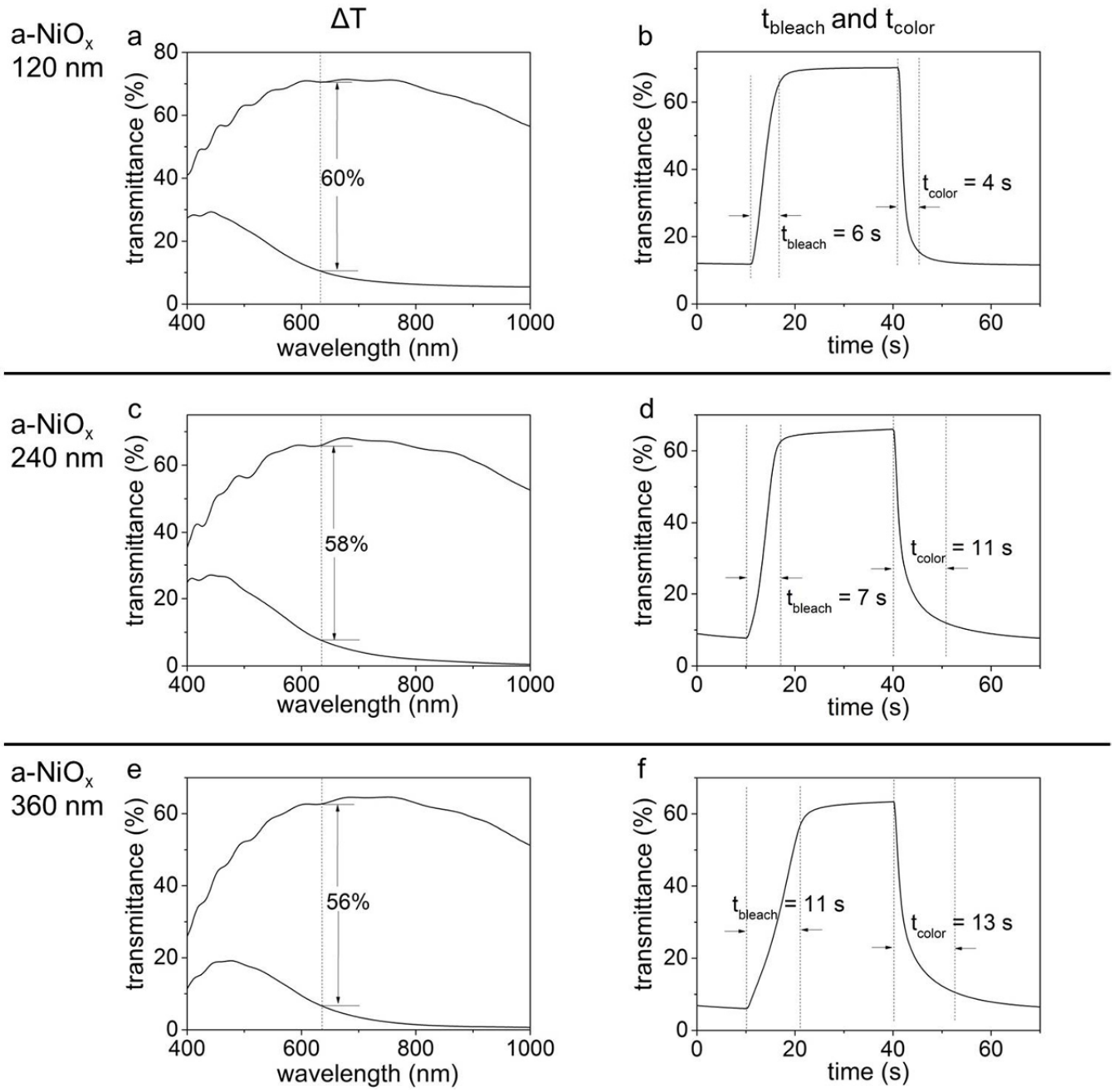

Figure S8. Thickness-dependent electrochromic performance, Related to Figures 3 and 4. Optical modulation and switching times of devices using a-NiO_x films with thicknesses of (a, b) 120 nm, (c, d) 240 nm, and (e, f) 360 nm as counter electrode materials. The 360-nm a-NiO_x film was made by 15 layers of coating and the thickness was calculated from the equation shown in Figure S7.

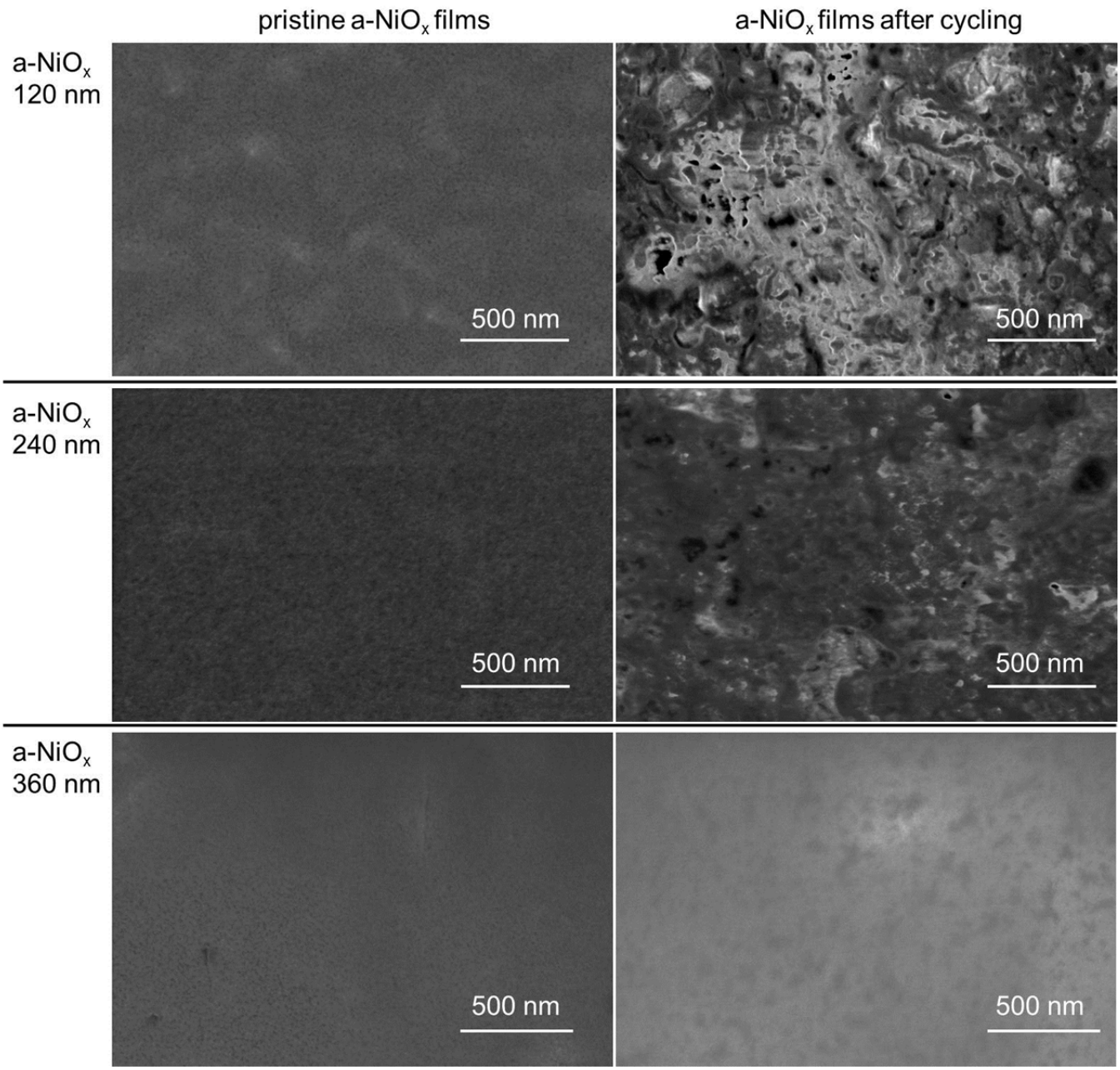

Figure S9. Influence of electrochromic cycling on the morphologies of a-NiO$_x$ films, Related to Figure 4. SEM images of a-NiO$_x$ films with different thicknesses before and after electrochromic cycling.

Transparent Methods

Materials

WCl_6 (99.99%), $NiCl_2 \cdot 6H_2O$ (99.9%), $LiClO_4$ (99.99%), PC (99.7%, anhydrous), 2-propanol (99.9%), and PMMA (M_w ~ 350000) purchased from Sigma-Aldrich were used directly without further purification. FTO-coated glass purchased from Hartford Glass (TEC7) was first cleaned by sequential ultrasonication in detergent solution (Extran 300, EMD), distilled water, acetone, and isopropanol, and then it was dried in N_2 flow and further subjected to UV-Ozone treatment for 30 min prior to use.

Film syntheses

In a typical synthesis of NiO_x film, a 0.25 M $NiCl_2$ aqueous solution prepared by dissolving 0.24 g (1.0 mmol) $NiCl_2 \cdot 6H_2O$ in 4 ml distilled water was spin-coated on FTO glass at 3000 rpm for 60 s (Laurell model WS-650MZ-23NPP-Lite). The resultant precursor thin films were subjected to UV (Atlantic Ultraviolet G18T5VH/U; λ_{max} = 185 nm) irradiation until complete decomposition was confirmed by tracking the chlorine content by XRF analysis. To produce multi-layer thin films, the spin-coating and UV light irradiation steps were repeated multiple times. The as-deposited films were annealed in an oven (Ney Vulcan 3-550) in air at different temperatures for 1 hr using a ramping rate of 10 °C/min.

The same procedures were used for synthesis of a-WO_3 films, except that a 0.25 M WCl_6 solution in isopropanol was used as precursor solution and UV irradiation time was 5 min. The as-deposited films were annealed in air at 100°C for 1 hr. WO_3 films with 5 layers of deposition were prepared and used in all devices throughout this work.

Electrolyte preparation

$LiClO_4$ and PMMA were dried at 100°C overnight, while PC was dried using a molecular sieve type-3A with a w/v of 20% overnight. The molecular sieves were activated by annealing at 300°C overnight before use. 0.53 g $LiClO_4$ was dissolved in 10 ml dry PC to form a 0.5 M solution. 1.34 g PMMA was then added to the $LiClO_4$-PC solution under magnetic stirring. The mixture was stirred and heated at 60°C on a hot plate for 16 hrs to form a colorless transparent gel.

Device assembly

Prior to device assembly, NiO_x films were prelithiated by electrochemical means using a conventional three electrode system with NiO_x films on FTO glass as the working electrode, Ag/AgCl as the reference electrode, Pt wire as the counter electrode and 1 M $LiClO_4$-PC as electrolyte. The lithium ions were intercalated into the NiO_x films by applying a potential of -1.5 V for 5 min.

Electrochromic devices were fabricated by placing a 2 × 2 cm square silicone rubber sheet (50 A, thickness = 1 mm; McMaster-CARR) with a centered hollow circle (diameter = 1.6 cm) on top of the prelithiated NiO_x film on FTO glass that serves as the counter electrode. The $LiClO_4$-PC-PMMA gel electrolyte was then drop-cast into the hollow circle. The FTO glass coated with a-WO_3 films (working electrode) was then laid on top of the silicon spacer to form a closed cell. Epoxy glue was used to seal the cell. The assembled devices were then heated at 60°C overnight before measuring the electrochromic performance. The assembled device had an active area of 2.0 cm^2.

Physical methods

An XRF analyzer (Thermo Fisher Scientific) was used to track chlorine in thin films. XPS analyses were carried out on a Leybold MAX200 spectrometer using Al Kα radiation. The pass energy was 192 eV for the survey scan and 48 eV for the narrow scan. Grazing incidence X-ray diffraction (GIXRD) experiments were performed with a Rigaku Smartlab diffractometer in parallel beam mode using Cu Kα radiation. Data were collected with a scan step of 0.04°, an incidence angle of 0.3°, and a scan rate of 3° min^{-1}. SEM images were acquired in secondary electron mode at 1 kV accelerating voltage on a Helios NanoLab 650 Focused Ion Beam SEM. To obtain cross-sectional images, FTO substrates coated with a-NiO_x films were cleaved in-house and the freshly broken edges were imaged at a tilt angle of 52°. The electrochromic properties of EC devices were measured with a PerkinElmer Lambda 35 UV-Vis spectrophotometer and a CHI660D potentiostat.